Syntheses, crystal structures and magnetic properties of complexes based on $[Ni(L\text{-}L)_3]^{2+}$ complex cations with dimethylderivatives of 2,2´-bipyridine and TCNQ

Juraj Černák [a*], Michal Hegedüs[a], Lucia Váhovská [a#], Juraj Kuchár [a], Daniela Šoltésová [b], Erik Čižmár [b], Alexander Feher [b], L. R. Falvello[c]

[a] P. J. Šafárik University in Košice, Faculty of Sciences, Institute of Chemistry, Department of Inorganic Chemistry, Moyzesova 11, 041 54 Košice, Slovakia

[b] P. J. Šafárik University in Košice, Faculty of Sciences, Institute of Physics, Park Angelinum 9, 041 54 Košice, Slovakia

[c] Departamento de Química Inorgánica and Aragón Materials Science Institute, University of Zaragoza–CSIC, E-50009 Zaragoza, Spain

Keywords: Nickel; tetracyanoquinodimethane; crystal structure; magnetic properties

Abstract

From the aqueous-methanolic systems $Ni(NO_3)_2$ – LiTCNQ – 5,5'-*dmbpy* and $Ni(NO_3)_2$ – LiTCNQ–4,4'-*dmbpy* three novel complexes $[Ni(5,5'\text{-}dmbpy)_3](TCNQ)_2$ (**1**), $[Ni(4,4'\text{-}dmbpy)_3](TCNQ)_2$ (**2**) and $[Ni(4,4'\text{-}dmbpy)_3]_2(TCNQ\text{-}TCNQ)(TCNQ)_2{\cdot}0.60H_2O$ (**3**), were isolated in single crystal form. The new compounds were identified using chemical analyses and IR spectroscopy. Single crystal studies of all samples corroborated their compositions and have shown that their ionic structures contain the complex cations $[Ni(5,5'\text{-}dmbpy)]^{2+}$ (**1**) or $[Ni(4,4'\text{-}dmbpy)]^{2+}$ (**2** and **3**). The anionic parts of the respective crystal structures **1**-**3** are formed by $TCNQ^{\cdot-}$ anion-radicals and in **3** also by a σ-dimerized dianion $(TCNQ\text{-}TCNQ)^{2-}$ with a C-C distance of 1.663(5) Å. The supramolecular structures are governed by weak hydrogen bonding interactions. The variable-temperature (2-300 K) magnetic studies of **1** and **3** confirmed the presence of magnetically active Ni(II) atoms with $S = 1$ and $TCNQ^{\cdot-}$ anion-radicals with $S = 1/2$ while the $(TCNQ\text{-}TCNQ)^{2-}$ dianion is magnetically silent. The magnetic behaviour was described by a complex magnetic model assuming strong antiferromagnetic interactions between some $TCNQ^{\cdot-}$ anion-radicals.

Present address of LV: University of Veterinary Medicine and Pharmacy in Košice, Department of chemistry, biochemistry and biophysics, Komenského 73, 041 81 Košice, Slovakia

1. Introduction

In the ongoing quest for new magnetic materials, especially those that behave as single-molecule magnets (SMM) (or single ion magnets and single chain magnets), a great variety of complexes based on 3d- and/or 4f-metals as carriers of unpaired spins are being studied extensively [1-4]. The carrier of the unpaired spin can alternatively be an organic radical, *e.g.*, based on 7,7',8,8'-tetracyano-*p*-quinondimethane (TCNQ) [5-6]. TCNQ (Scheme 1) is a very versatile chemical species, as it can adopt different electronic states such as anion-radical $TCNQ^{\cdot-}$; but other forms of TCNQ have been identified, including π- and σ- dimerized forms [7-10]. TCNQ in the anion-radical form can act as a σ-donor ligand in terminal or bridging fashions (linking up to four metal centers), or can be present in the structure as a counter anion, often in a dimerized form [11-14]. TCNQ in combination with magnetically active transition metals sometimes displays spectacular magnetic behavior [15-18]. Moreover, materials based on TCNQ have generated high interest due to their electrical conductivity [19-22], or their gas, photo- and immunosensing properties [23-25]; their use in catalysis [26] or as cathode materials [27] has been reported, too.

A variety of octahedral Ni(II) complexes containing TCNQ have been synthesized and structurally characterized to date [11, 28-29]. With bidentate *N–N* donor chelating ligands L-L, few Ni(II) complexes containing $[Ni(L\text{-}L)_3]^{2+}$ cations have been characterized, *e.g.*, $[Ni(en)_3](TCNQ)_2$ (*en* = ethylenediamine) [7], $[Ni(abpt)_2(TCNQ)_2]$ (*abpt* = 4-amino-3,5-di-2-pyridyl-4H-1,2,4-triazole) [13] or $[Ni(bpy)_3](TCNQ)_4\cdot 2Me_2CO$ [8]. In our search for materials containing two different spin carriers [30], we have synthesized Ni(II) (S = 1) complexes with TCNQ. Recently, we have elucidated the ionic crystal structure of $[Ni(bpy)_3](TCNQ)_2\cdot 3H_2O$ containing π- as well as σ-dimerized TCNQs [31].

As a continuation of this line of research we have used 5,5'-*dmbpy* and 4,4'-*dmbpy* (*dmbpy* = dimethyl-2,2´-bipyridine, Scheme 1) as blocking ligands. We present here our results on the syntheses, spectroscopic characterization, crystal structures and magnetic properties of $[Ni(5,5'\text{-}dmbpy)_3](TCNQ)_2$ (**1**), $[Ni(4,4'\text{-}dmbpy)_3](TCNQ)_2$ (**2**) and $[Ni(4,4'\text{-}dmbpy)_3]_2(TCNQ\text{-}TCNQ)(TCNQ)_2\cdot nH_2O$ (n = 0.60) (**3**).

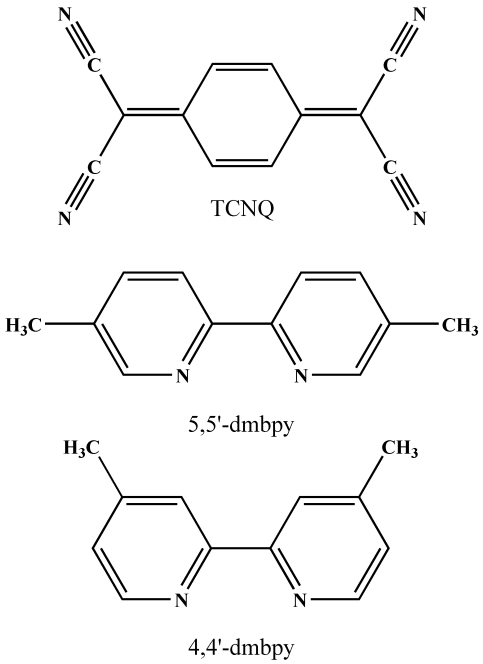

Scheme 1 Chemical structures of TCNQ, 5,5ˈ-*dmbpy* and 4,4ˈ-*dmbpy*.

2. Experimental

2.1. Materials

$Ni(NO_3)_2 \cdot 6H_2O$, TCNQ and 4,4ˈ- and 5,5ˈ-dimethyl-2,2´-bipyridines were purchased from commercial sources and used as received. LiTCNQ was prepared according to the published method [32].

2.2. Syntheses

[Ni(5,5ˈ-*dmbpy*)$_3$](TCNQ)$_2$ (1). A solution of LiTCNQ (0.3 mmol, 63.3 mg) in methanol (5 ml) was added to a mixture of $Ni(NO_3)_2 \cdot 6H_2O$ (0.15 mmol, 43.6 mg) and 5,5'-*dmbpy* (0.45 mmol, 82.9 mg) in methanol (5 ml). The mixture was stirred for 15 min. at room temperature, and the resulting blue-green precipitate of [Ni(5,5'-*dmbpy*)$_3$](TCNQ)$_2$ was filtered off, washed with methanol and diethylether and dried in air. Yield: 83 %.

Single crystals suitable for X-ray study were obtained by recrystallization of the microcrystalline sample from hot methanol. After slow cooling of a boiling methanolic solution, dark green prisms of [Ni(5,5'-*dmbpy*)$_3$](TCNQ)$_2$ were immediately formed; these were filtered

off, washed with methanol and ether and dried in air. We note that rapid cooling of the boiling methanolic solution did not yield crystals. Anal. Found (Calcd) % for ($C_{60}H_{44}N_{14}Ni$): C, 71.31 (70.67); H, 4.42 (4.35); N, 19.30 (19.23). IR (ν(CN), KBr, in cm^{-1}): 2178(vs) and 2152(s).

[Ni(4,4'-*dmbpy*)$_3$](TCNQ)$_2$ (2). Solid 4,4'-*dmbpy* (0.225 mmol) was added to a solution of $Ni(NO_3)_2 \cdot 6H_2O$ (0.075 mmol) in methanol (2 ml). The mixture was stirred and heated until a homogenous light purple solution resulted. A boiling solution of LiTCNQ (0.15 mmol) in methanol (2 mL) was poured into the hot solution of the nickel salt under constant stirring. The resulting dark green solution was allowed to cool to room temperature. A crystalline mixture of **2** and **3** (parallelepipeds and needles, respectively) was obtained. The crystals were filtered off and washed with a small amount of methanol and diethyl ether. Well-shaped monoclinic parallelepipeds of the product [Ni(4,4'-*dmbpy*)$_3$](TCNQ)$_2$ (**2**) were manually separated. Anal. Found (Calcd) % for ($C_{60}H_{44}N_{14}Ni$): C, 70.55 (70.67); H, 4.59 (4.35); N, 18.89 (19.23). IR (ν(CN), KBr, in cm^{-1}): 2180(vs) and 2153(s).

[Ni(4,4'-*dmbpy*)$_3$]$_2$(TCNQ-TCNQ)(TCNQ)$_2$·*n*H_2O (*n* = 0.60) (3). Solid 4,4'-*dmbpy* (0.225 mmol) was added to a solution of nickel(II) nitrate hexahydrate (0.075 mmol) in methanol (2 mL). The mixture was stirred and heated up to 65 °C until a homogenous light purple solution resulted. A dark green solution of LiTCNQ (0.15 mmol) in methanol (2 mL) of the same temperature was added into the solution of the nickel salt. The resulting solution was immediately enclosed in a 5 mL vial and it was cooled down to room temperature (8.75 deg/hour) in a programmable drying-oven. Only dark green needle-like crystals of [Ni(4,4'-*dmbpy*)$_3$]$_2$(TCNQ-TCNQ)(TCNQ)$_2$·*n*H_2O (n = 0.60) were obtained. The needle-like crystals were filtered off, washed with a small volume of methanol and diethylether. Yield: 61 %. Anal. Found (Calcld) % for ($C_{120}H_{88}N_{28}Ni_2 \cdot 0.60H_2O$): C, 70.49 (70.29); H, 4.33 (4.39); N, 18.95 (19.13). IR (ν(CN), KBr, in cm^{-1}): 2177(vs), 2152(m) and 2138(m).

2.3. Instrumental methods

Elemental analyses of C, H and N were performed on a CHNOS Elemental Analyzer vario MICRO (Elementar Analysensysteme GmbH). The infrared spectra in the range 4000–400 cm^{-1} were recorded on a Nicolet 6700 FT-IR spectrophotometer (Thermo Scientific) using the KBr method.

2.4 X-ray structure analysis

The single crystal X–ray experiment on [Ni(5,5'-*dmbpy*)$_3$](TCNQ)$_2$ was done on a four-circle κ-axis Xcalibur2 diffractometer equipped with a Sapphire2 CCD detector (Oxford Diffraction) and with graphite-monochromated Mo Kα radiation (λ=0.71073 Å) at 170(2) K. The CrysAlis software package [33] was used for data collection and reduction. Analytical numeric absorption correction was done using a multifaceted crystal model [34]. The crystal structure was solved by direct methods (SHELXS) and refined using SHELXL-2014/7 [35-36], incorporated in the WinGX program package [37]. Hydrogen atoms in the ligands were placed in calculated positions and allowed to ride on the parent atoms with isotropic thermal parameters tied with the parent atoms (U_{iso}(H) = 1.2U_{eq}(CH$_2$), U_{iso}(H) = 1.5U_{eq}(CH$_3$)).

Single-crystal X-ray data [Ni(4,4'-*dmbpy*)$_3$](TCNQ)$_2$ (**2**) and [Ni(4,4'-*dmbpy*)$_3$]$_2$(TCNQ-TCNQ)(TCNQ)$_2$·nH$_2$O (**3**) were collected on an Oxford Diffraction Xcalibur diffractometer equipped with a Sapphire3 CCD detector and a graphite monochromator utilizing Mo-Kα radiation (λ = 0.71073 Å). Analytical numerical absorption correction using a multifaceted crystal model was used for **2** [33-34] while the data for **3** were corrected for absorption using ABSPACK (multiscan technique) [38-39]. The structures were solved by SIR2014 [40] and refined against F^2 using full-matrix least squares methods with the program SHELXL-2014/7 [36]. Anisotropic displacement parameters were refined for all non-hydrogen atoms. The hydrogen atoms bonded to carbon and oxygen atoms were included at idealized positions and refined as riders with isotropic displacement parameters assigned as *x* times the U_{eq} values of their corresponding bonding partners, with *x* = 1.5 for CH$_3$ and *x* = 1.2 for all others. For **2**, voids were found containing residual electron density. This was modelled using the SQUEEZE procedure [41], which yielded 17 electrons per void; we note that this value may correspond to partial occupancy of the voids by methanol solvent molecules.

The structural figures were drawn using Diamond [42]. The crystal data and final parameters of the structure refinements are summarized in Table 1, while selected geometric parameters are given in Table 2. Possible hydrogen bonds are gathered in Table 3.

Table 1 Crystal data and structure refinement for **1-3**.

	1	**2**	**3**
Empirical formula	C60 H44 N14 Ni	C61 H48 N14 Ni O	C120 H89.20 N28 Ni2 O0.60
Formula weight	1019.78	1051.84	2050.41
Wavelength [Å]	0.71073 Å	0.71073 Å	0.71073 Å
Crystal system	Monoclinic	Monoclinic	Triclinic
Space group	$P2_1/c$	$C2/c$	P-1
T [K]	173(2)	100(2)	100(2)
Unit cell dimensions [Å, °]	a = 11.3629(5)	a = 18.0257(4)	a = 14.1556(6)
	b = 10.2040(4)	b = 17.1404(4)	b = 20.2782(11)
	c = 44.6148(15)	c = 18.7487(5)	c = 20.9469(9)
	β = 91.211(3)	β = 108.693(3)	α = 63.100(5)
			β = 73.750(4)
			γ = 87.651(4)
Volume [Å^3]	5171.8(4)	5487.2(2)	5122.2(5)
Z	4	4	2
Density (calculated) [g.cm^{-3}]	1.3097	1.273	1.329
Absorption coefficient [mm^{-1}]	0.430	0.409	0.435
Crystal dimensions [mm^3]	0.42 x 0.21 x 0.11	0.90 x 0.36 x 0.32	0.026 x 0.153 x 0.504
θ range for data collection [°]	2.85 to 26.00	3.30 to 27.50	2.72 to 26.41
Index ranges	–14 ≤ h ≤ 13	–23 ≤ h ≤ 23	–17 ≤ h ≤ 17
	–12 ≤ k ≤ 11	–22 ≤ k ≤ 21	–25 ≤ k ≤ 25
	–35 ≤ l ≤ 55	–24 ≤ l ≤ 24	–26 ≤ l ≤ 24
Reflections coll./ obs.	10136/7662	6201/5098	20958/13719
Absorption correction	Analytical	Analytical	Multi-scan
T_{min}/T_{max}	0.890/0.962	0.811/0.898	0.814/1.000
Completeness to 2θ*(max)*	0.998	0.984	0.995
R1 obs. [I > 2σ(I)]	0.058	0.0442	0.0579
all data	0.0849	0.0574	0.1006
wR2 obs. [I > 2σ(I)]	0.1208	0.1033	0.1299
all data	0.1331	0.1107	0.1536
Goodness-of-fit, *S* (all/obs.)	1.090/1.090	1.035/1.035	1.011/1.011
Largest diff. peak and hole [e.Å^{-3}]	0.65 and -0.47	0.29 and -0.29	0.51 and -0.63

2.5 Magnetic studies

Magnetic properties were investigated using a Quantum Design MPMS3. Measurements of magnetic susceptibility were performed in a magnetic field 100 mT in zero-field cooled (ZFC) and field cooled (FC) regimes at temperatures from 1.8 to 300 K for compound **1** and 5 – 300 K for compound **3**. The core diamagnetic contribution to the magnetic susceptibility estimated using Pascal's constants [43] and the typical value of the temperature-independent paramagnetic susceptibility of Ni^{2+} ions (100 x 10^{-6} emu/mol) were subtracted from the raw data. The field dependence of magnetization was measured in magnetic fields up to 7 T at temperatures of 1.8 K and 5 K for compound **1** and at temperatures of 5 K and 15 K for compound **3**.

2.6 Computational details

Ab initio calculations were performed using the ORCA 4.0.1 computational package [44]. The zeroth-order regular approximation (ZORA) together with the scalar relativistic contracted version of basis functions Def2-TZVP(-f) was used. The calculations of zero-field splitting (ZFS) parameters were based on state-averaged complete-active-space self-consistent field (SA-CASSCF) wave functions followed by N-electron valence second-order perturbation theory (NEVPT2). The active spaces of the CASSCF calculations on metal-based d-orbitals were defined as CAS(8,5) for Ni(II). The state averaged approach was used with all 10 triplet states and 15 singlet states equally weighted. The calculations utilized the RI approximation with appropriate decontracted auxiliary basis set and the chain-of-spheres (RIJCOSX) approximation to exact exchange. Increased integration grids (Grid4) and tight SCF convergence criteria were used. The ZFS parameters were calculated through the quasi-degenerate perturbation theory in which an approximation to the Breit-Pauli form of the spin-orbit coupling operator and the effective Hamiltonian theory were utilized.

3. Results and discussion

3.1. Syntheses and identification

Reaction of LiTCNQ with nickel nitrate in the presence of 5,5'-*dmbpy* in methanolic solution yielded the complex $[Ni(5,5'\text{-}dmbpy)_3](TCNQ)_2$ (**1**). From the analogous system with

4,4'-*dmbpy* two different complexes could be isolated depending on the cooling regime of the hot methanolic reaction solutions: when the reaction solution was left to cool freely to room temperature, a mixture of both **2** and **3** in single crystal form (parallelepipeds and needles) was obtained, while slow controlled cooling yielded only needles of **3**. The purity and chemical identity of the samples were corroborated by elemental analyses and confirmed by single crystal X-ray studies (see below). We note that Melby *et al*. [32] reported the synthesis and characterization of analogous complexes [Ni(*phen*)$_3$](TCNQ)$_2$·6H$_2$O and Ni(*phen*)$_2$](TCNQ)$_2$·6H$_2$O (*phen* = 1,10-phenanthroline) while Ni(II) complexes with *bpy* in the form of acetone and water solvates, [Ni(*bpy*)$_3$](TCNQ)$_4$·2Me$_2$CO [8] and [Ni(*bpy*)$_3$](TCNQ)$_2$·3H$_2$O [31], respectively, were recently prepared and structurally characterized.

The IR spectra of **1–3** contain typical absorption bands due to ν(C≡N) stretching vibrations from the TCNQ species (Fig. 1). A common feature of the spectra of all three complexes is a very strong ν(C≡N) peak positioned at around 2178 cm^{-1} and an additional weaker one at approximately 2150 cm^{-1}. In the spectrum of **3**, a third peak is observed at 2138 cm^{-1} probably due to the presence of two different TCNQ species in the structure. In the IR spectrum of [Ni(*dien*)$_2$](TCNQ)$_2$ (*dien* = 1,4,7-triazaheptane) with non-coordinated TCNQ the corresponding peaks were found at very similar values of 2178 and 2156 cm^{-1} [11]. On the other hand, in the spectrum of [Ni(*trien*)(TCNQ)$_2$] (*trien* = 1,4,7,10-tetraazadecane) with monodentate N-coordinated TCNQ, besides the absorption bands at 2176, 2163 and 2157 cm^{-1} two additional absorption bands at higher wavenumbers (2202 and 2190 cm^{-1}) were observed [11]; so the absence of the absorption bands above 2190 cm^{-1} in the IR spectra of our compounds excludes the direct coordination of TCNQ to the Ni(II) center; this assumption was confirmed by the crystal structures (see below).

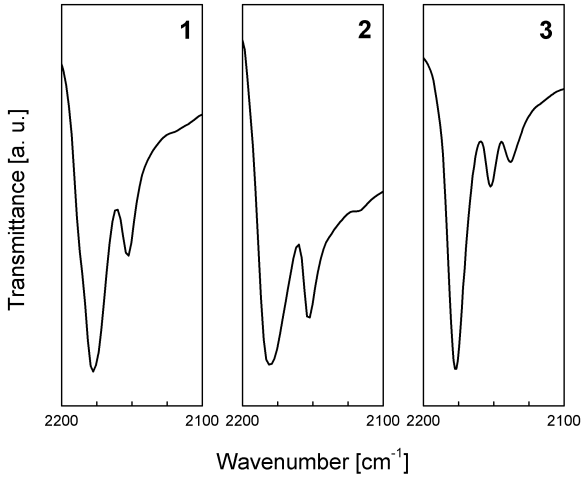

Fig. 1 IR spectra of complexes **1** (left), **2** (middle) and **3** (right) in the region of the stretching vibrations of the cyanide groups.

3.2. Crystal structures

The crystal structure of [Ni(5,5'-*dmbpy*)$_3$](TCNQ)$_2$ (**1**) is ionic and is formed of [Ni(5,5´-*dmbpy*)$_3$]$^{2+}$ complex cations and two crystallographically independent TCNQ$^{\cdot-}$ anion-radicals, TCNQ1 containing N7 and TCNQ2 containing N11 (Fig. 2, Fig. 3). Similar ionic structures were observed for some other nickel complexes with TCNQ, *e.g.*, [Ni(*dien*)$_2$](TCNQ)$_2$ (*dien* = 1,4,7-triazaheptane) [11] or [Ni(*terpy*)$_2$](TCNQ)$_2$ (*terpy* = 2,2':6',2"-terpyridine) [28]. The Ni(II) central atom within the complex cation of **1** is hexacoordinated by three chelating 5,5'-*dmbpy* ligands. It is interesting to note that although the [Ni(*bpy*)$_3$]$^{2+}$ complex cation has been described many times in the literature, [*e.g.*, 45-46], this is, according to a search in the CSD [47], not the case for [Ni(5,5'-*dmbpy*)$_3$]$^{2+}$. To our knowledge, up to now, this complex cation has been structurally characterized only scarcely, *e.g.*, in [Ni(5,5'-*dmbpy*)$_3$]$_2$[$V_2W_4O_{19}$]·6H_2O [48]. The observed Ni-N bonds in **1** lie in the narrow range 2.080(2)-2.099(2) Å, and the bite angles N-Ni-N exhibit values in the range 78.79(9)-79.07(9)° (Table 2). These values as well as the other geometric parameters associated with this complex cation (Table 2) are close to those reported for [Ni(5,5'-*dmbpy*)$_3$]$_2$[$V_2W_4O_{19}$]·6H_2O [48].

One of the two TCNQ$^{\cdot-}$ anion-radicals, namely TCNQ1 (containing N7) (Fig. 2), is π-dimerized with its symmetry (-1) related species (Fig. 4). The interplanar distance 3.005 Å

between the two quinoide rings, which are parallel as required by -1 symmetry, is relatively short. A similar short distance of 3.03 Å between the neighbouring molecular planes of TCNQ was observed in {[Mn(4,4'-*bpy*)(η^1-TCNQ)$_2$(CH$_3$OH)$_2$]TCNQ}·0.5H$_2$O [49], while longer distances were observed in analogous [Ni(*dien*)$_2$](TCNQ)$_2$ (interplanar distance is 3.23 Å) [11] or [Ni(*terpy*)$_2$](TCNQ)$_2$ with the shortest interplanar distance of 3.28 Å [28]. The calculated value of the longitudinal offset of 2.119 Å with zero transversal offset for the two symmetry related TCNQ1s is in excellent agreement with the statistically observed value of 2.1 Å for "ring-external bond" type overlap [50]. As can be seen from Fig. 3 the π-dimerized TCNQ1 species are placed in a chain-like stacking arrangement running along the *b* axis with a longer nearest approach of 3.624 Å between the π-dimerized TCNQ1 pairs (Fig. S1).

The bond lengths in TCNQ species can be used for estimation of the charge localized on it as its presence manifests itself by the shift of the relevant geometric parameters of the TCNQ molecule toward its aromatization [51]. Using the Kistenmacher relationship ζ = A[c/(b+d)] + B (A = -41.667, B = 19.833, and b, c and d are the average bond distances within the TCNQ molecule, see Scheme 2) [49, 51] the values of ζ were calculated.

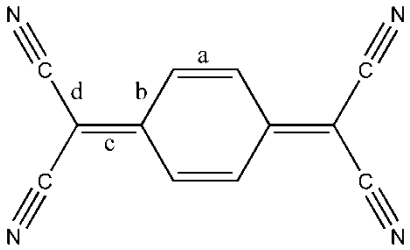

Scheme 2 TCNQ molecule and the meaning of b, c and d values for the Kistenmacher relationship.

The obtained values of ζ1 (for the TCNQ1 molecule) and ζ2 (TCNQ2) are -0.72 and -1.06. As the complex cation containing Ni(II) and neutral ligands has a charge 2+ iwe would expect both TCNQ molecules to have charge -1. While the result of the calculation for the TCNQ2 species corresponds well to this expectation, in the case of TCNQ1 a lower value was obtained; the observed difference may be the consequence of the rather strong π-dimerization of this species.

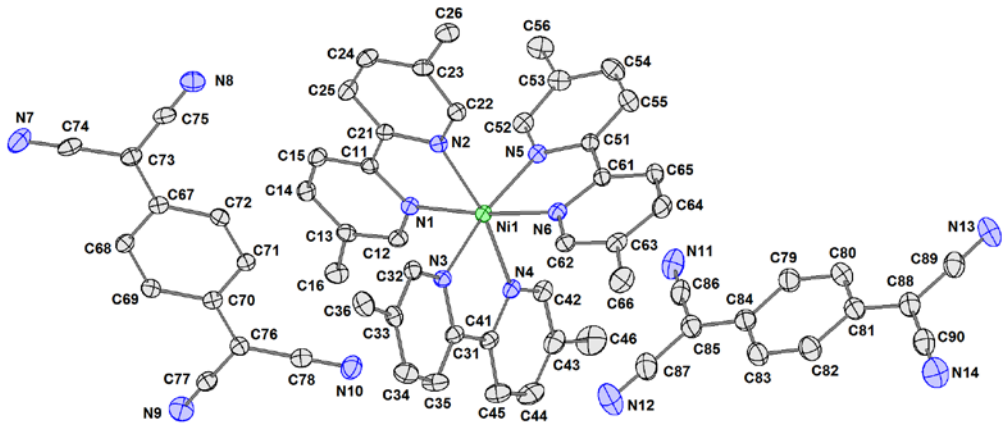

Fig. 2 Molecular structure of **1** including atom numbering scheme. The thermal ellipsoids are drawn at the 30 % probability level. Hydrogen atoms are omitted in the sake of clarity.

Table 2 Selected geometric parameters [Å, °] for **1**.

Ni1-N1	2.091(2)	N1-Ni1-N2	78.70(9)
Ni1-N2	2.080(2)	N3-Ni1-N4	79.07(9)
Ni1-N3	2.083(2)	N5-Ni1-N6	78.77(9)
Ni1-N4	2.082(2)	N11-C86	1.153(4)
Ni1-N5	2.077(2)	N12-C87	1.147(5)
Ni1-N6	2.099(2)	N13-C89	1.156(4)
N7-C74	1.148(4)	N14-C90	1.149(4)
N8-C75	1.154(4)		
N9-C77	1.142(4)		
N10-C78	1.146(4)		

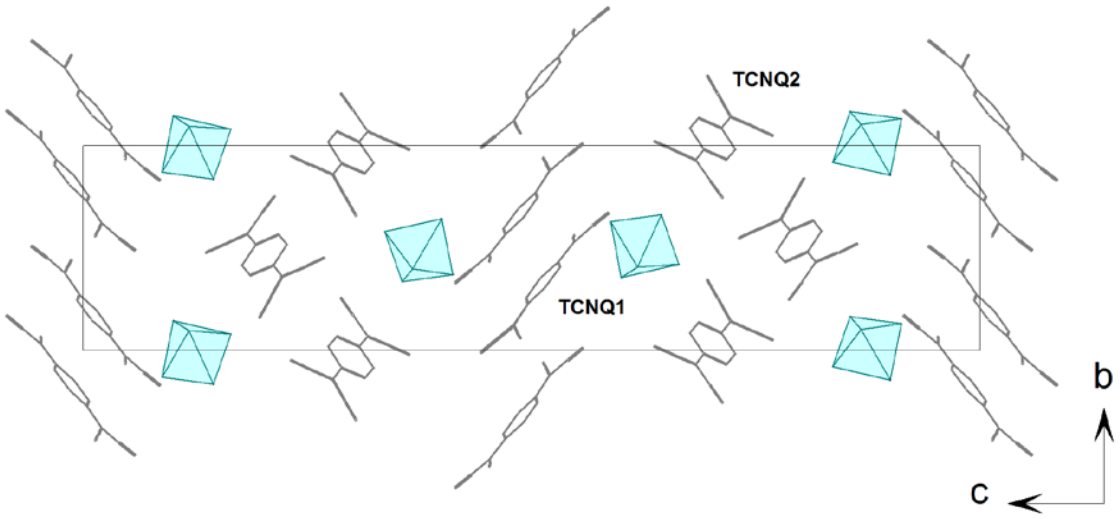

Fig. 3 Packing view of the crystal structure of **1**. The $[Ni(5,5'\text{-}dmbpy)_3]^{2+}$ complex cations are displayed as light-blue octahedra. TCNQ1 and TCNQ2 are the crystallographically independent $TCNQ^{\cdot-}$ anion-radicals involving N7 and N11, respectively.

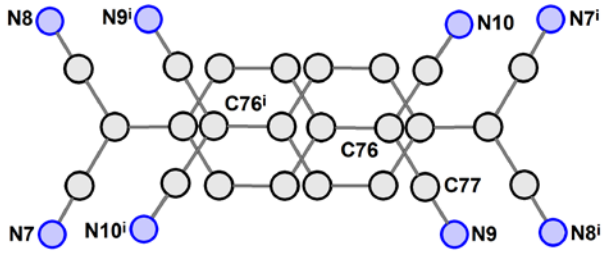

Fig. 4 π-Dimerization of TCNQ1 in **1** with its inversion-related congener, $TCNQ1^{i}$. Symmetry code: i: 2-x, 1-y, 1-z.

There are no classical hydrogen bonds in **1** so the packing of **1**, besides ionic forces, is governed by weaker C-H···N hydrogen bonding interactions which are gathered in Table S1, and, in addition, by the already mentioned stacking forces between TCNQ1 anion-radicals. The weak hydrogen bonding interactions lead to a 2D supramolecular arrangement of complex cations and TCNQ1 anion-radicals running along the *a* axis (Fig. S2).

The crystal structures of $[Ni(4,4'\text{-}dmbpy)_3](TCNQ)_2$ (**2**) and $[Ni(4,4'\text{-}dmbpy)_3]_2(TCNQ\text{-}TCNQ)(TCNQ)_2\cdot 0.60H_2O$ (**3**) are ionic and contain the same $[Ni(4,4'\text{-}dmbpy)_3]^{2+}$ complex cations (Fig. 5, Fig. 6). We note that in **3** there are two crystallographically independent

complex cations. The nickel(II) central atoms within the complex cations in both **2** and **3** are hexacoordinated by three chelating 4,4´-*dmbpy* ligands. The same complex cation was found in [Ni(4,4'-*dmbpy*)$_3$](Sb$_3$S$_5$)$_2$ [52]. The observed Ni-N bonds in **2** lie in the range 2.0686(15) - 2.1019(15) Å (2.059(2) - 2.110(2) Å in **3**); the bite angles N-Ni-N exhibit values of 78.37(6) and 78.85(8)° which are almost identical to the corresponding values in **3** (78.15(9) - 78.84(9)°) (Table 3, Table 4). These geometric parameters are also in line with those reported for [Ni(4,4'-*dmbpy*)$_3$](Sb$_3$S$_5$)$_2$ [52].

The anionic parts of **2** and **3** are different. In **2**, contrary to what is found for **1**, the TCNQ·$^-$ anion-radicals are not π-dimerized. Although the two closest TCNQ·$^-$ anion-radicals are parallel and related by an inversion centre (-1) they are displaced away from each other, and the shortest distance between the symmetry related species is represented by the contact N5···C30^{ii} (ii: 1-x, 1-y, 1-z) of 3.476(6) Å (Fig. 7). The presence of the negative charge -1 on the TCNQ·$^-$ anion-radical in **2** is supported by the calculations using the Kistenmacher relationship [51] which yields a value of ζ = -0.93 which is close to the expected value.

There are no classical hydrogen bonds in **2** so the packing of its structure (Fig. 8) is governed, besides by ionic forces, by a weaker C4-H4···N7^{iii} hydrogen bonding interaction with distance C4···N7^{iii} of 3.448(5) Å and angle C4-H4-N7^{iii} of 160° (symmetry code iii: x-0.5, 0.5-y, z-0.5). This weak hydrogen bonding interaction leads to the formation of a trinuclear supramolecular unit built up of one complex cation and two TCNQ anion-radicals (Fig. S3).

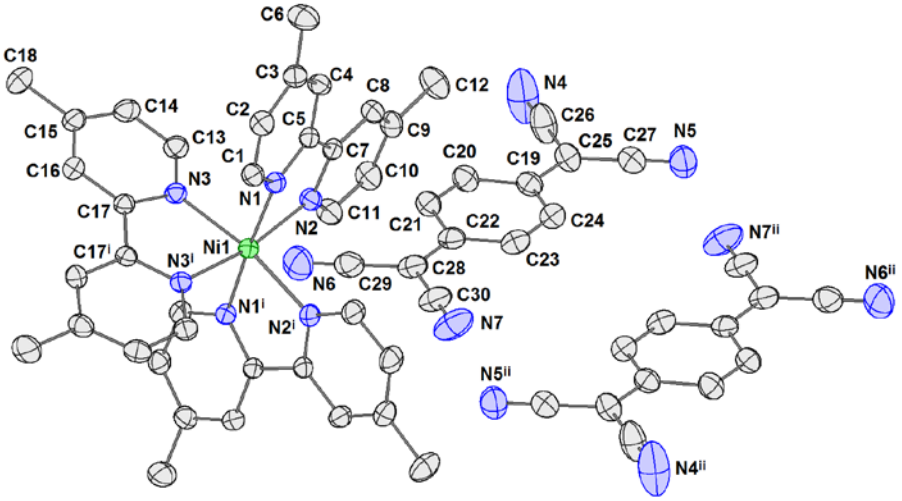

Fig. 5 Molecular structure of **2** including the atom numbering scheme. The thermal ellipsoids are drawn at 30 % probability level. Hydrogen atoms are omitted for the sake of clarity. Symmetry codes: i: 1-x, y, 0.5-z; ii: 1-x, 1-y, 1-z.

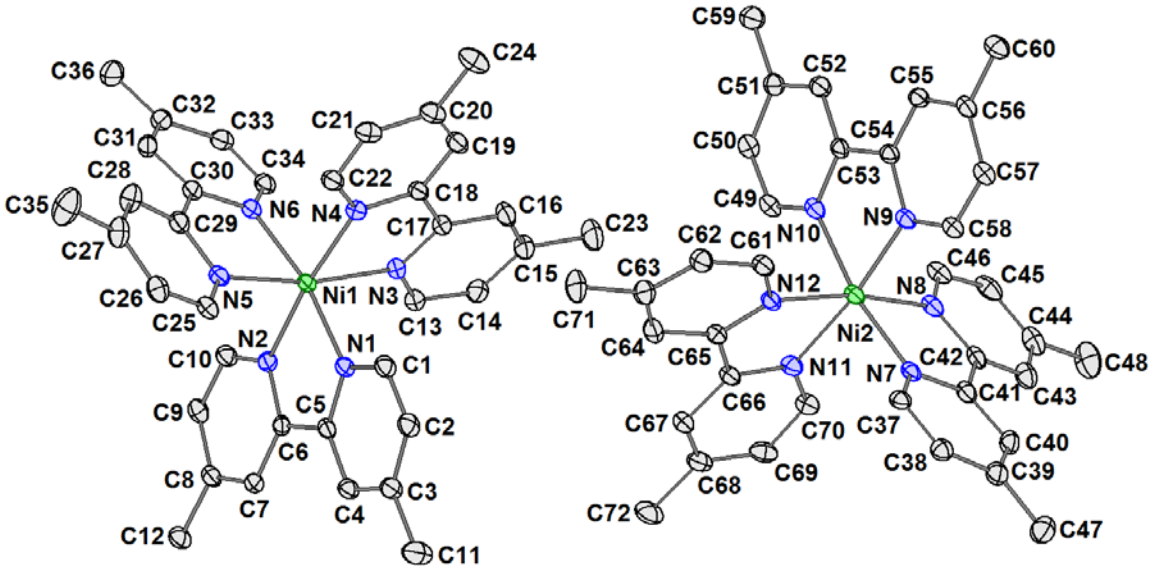

Fig. 6 View of the two crystallographically independent complex cations in **3** displaying the atom numbering scheme. The thermal ellipsoids are drawn at 30 % probability level.

Table 3 Selected geometric parameters [Å, °] for **2**.

Ni1-N1	2.1019(15)	N1-Ni1-N2	78.37(6)
Ni1-N2	2.0686(15)	N3-Ni1-N3^{i}	78.85(8)
Ni1-N3	2.0796(15)		
N4-C26	1.137(4)		
N5-C27	1.140(3)		
N6-C29	1.141(3)		
N7-C30	1.140(3)		

Symmetry code: i: -x + 1, y, -z + 0.5

Table 4 Selected geometric parameters [Å, °] for **3**.

Ni1-N1	2.061(2)	N1-Ni1-N2	78.67(9)
Ni1-N2	2.084(2)	N3-Ni1-N4	78.52(9)
Ni1-N3	2.068(2)	N5-Ni1-N6	78.79(9)
Ni1-N4	2.092(2)	N7-Ni2-N8	79.41(9)
Ni1-N5	2.087(2)	N9-Ni2-N10	78.84(9)
Ni1-N6	2.077(2)	N11-Ni2-N12	78.13(9)
Ni2-N7	2.065(2)	C95-N20	1.156(4)
Ni2-N8	2.075(2)	C96-N19	1.158(4)
Ni2-N9	2.077(2)	C97-N22	1.171(5)
Ni2-N10	2.079(2)	C98-N21	1.164(5)
Ni2-N11	2.109(2)	C107-N23	1.161(5)
Ni2-N12	2.066(2)	C108-N24	1.167(5)
C73-N13	1.158(4)	C109-N26	1.153(5)
C74 N14	1.165(4)	C110-N25	1.147(4)
C84 N16	1.147(4)	C120 N28	1.156(4)
C85 N17	1.123(4)	C82-C87	1.663(5)
C86 N18	1.130(4)		

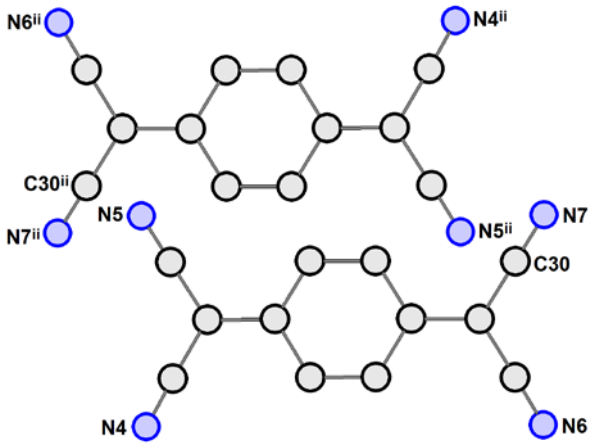

Fig. 7 Parallel arrangement of the neighbouring $TCNQ^{\cdot-}$ anion-radicals in **2** related by a center of symmetry. The shortest distance of 3.476(6) Å is represented by the contact $C30\cdots N5^{ii}$. Symmetry code: ii: 1-x, 1-y, 1-z.

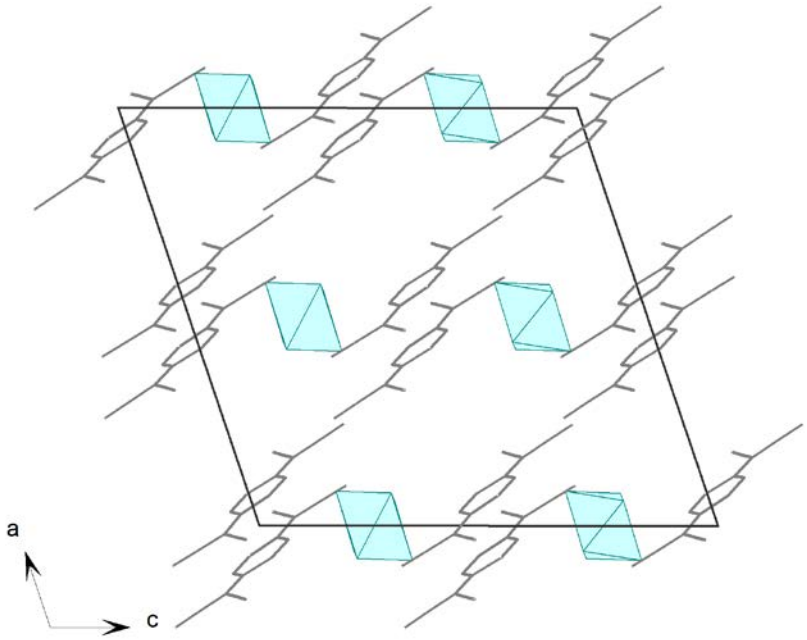

Fig. 8 Packing diagram of the structure of complex **2** viewed along the *b* axis. For clarity the complex cations are represented by light-blue octahedra and $TCNQ^{\cdot -}$ anion-radicals are depicted using a wire model.

In the crystal structure of **3**, there are two crystallographically independent $TCNQ^{\cdot -}$ anion-radicals as well as a σ–dimerized $(TCNQ\text{-}TCNQ)^{2-}$ dianion (Fig. 9). Both $TCNQ^{\cdot -}$ anion-radicals TCNQ1 and TCNQ2 (TCNQ1 is the anion-radical containing atom N21, TCNQ2 is the anion-radical containing atom N25) exhibit unexceptionalgeometric parameters (Table 4) and their negative (-1) charge is supported by the calculated values of ζ1 = -0.94 for TCNQ1 and ζ2 = -0.90 for TCNQ2 using the Kistenmacher relationship [51].

The formation of the σ–dimerized $(TCNQ\text{-}TCNQ)^{2-}$ dianion can be considered as a tendency toward pairing of the two isolated spins. Taking into account the different cooling regimes during the syntheses leading to **2** and **3** (see Experimental part) our conjecture is that **2** is the product of the kinetically controlled reaction while **3** is the product of the thermodynamically controlled reaction manifesting itself by partial completion of the σ-dimerization reaction. A similar situation was observed in $[Ni(bpy)_3](TCNQ)_2{\cdot}3H_2O$ [31]. Within the σ-dimerized dianion in **3** the observed C-C bond length is 1.663(5) Å; this value is somewhat longer than a normal C-C single bond but almost identical to the value of 1.645(7) Å that was found in $[Fe(phen)_3](TCNQ)_2$ [28]. We note that in the case of such σ-dimerization

the reported values for C-C bonds range from 1.612 Å in polymeric *catena*-[Zn(*bipy*)(μ_4-TCNQ-TCNQ)]$_n$·*n*(*p-xy*) (*bipy* = 4,4-bipyridine, *p-xy* = *p*-xylene) [53] to 1.673 Å in [Pt(*bpy*)$_2$](TCNQ-TCNQ), with an ionic structure [54].

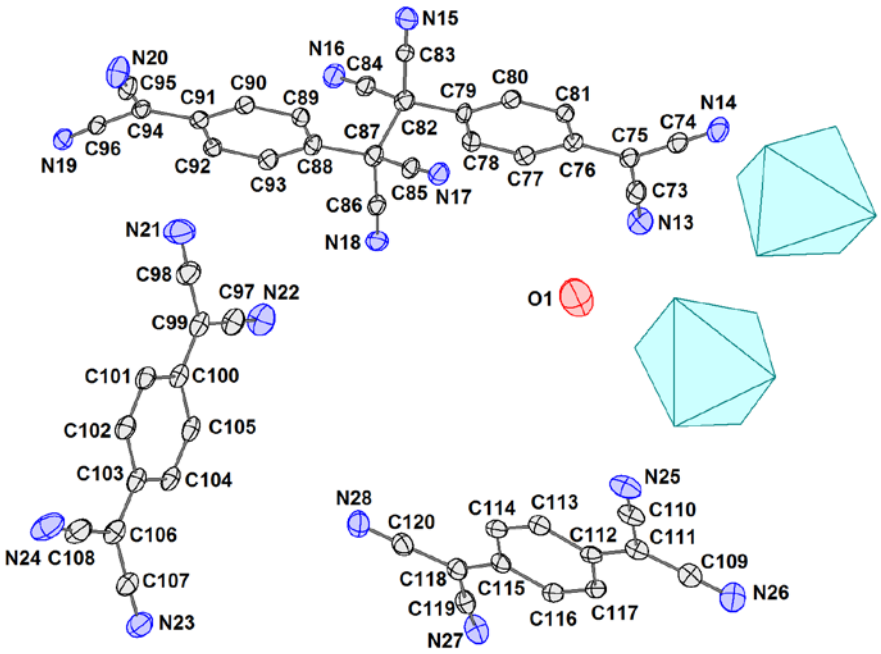

Fig. 9 View of the σ-dimerized dianion (TCNQ-TCNQ)$^{2-}$ and two TCNQ·$^-$ anion radicals in the crystal structure of **3** along with the atom numbering scheme. The positions of the two complex cations are shown only as light-blue octahedra. The thermal ellipsoids are drawn at 30% probability level.

In the unit cell of complex **3** (Fig. 10) a solvate water molecule O1 with partial occupancy (s.o.f. = 0.60) is present, too. It is only weakly bound to the remaining parts of the structure; it is involved in a weak hydrogen bonding interaction C26^{i}-H26^{i}···O1 (i: 1-x, 1-y, 1-z) (Table S2) and there are two additional short O1···N distances with N13 (3.0711(2) Å) and N21^{ii} (ii: 2-x, 1-y, 1-z) 3.3861(2) Å), suggesting possible formation of hydrogen bonds with the TCNQ units (Fig. 11). The stability of the structure is enhanced by several weak

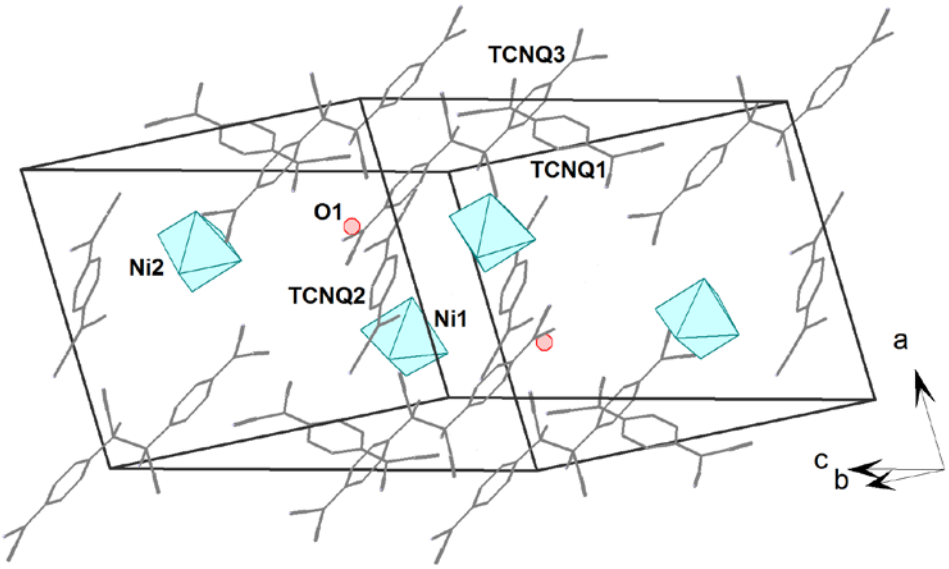

Fig. 10 Packing diagram of **3**. The light blue octahedra show the positions of the complex cations containing Ni1 and Ni2 central atoms. TCNQ1 is the anion-radical containing atom N21, TCNQ2 is the anion-radical containing atom N25 and TCNQ3 is the $(TCNQ\text{-}TCNQ)^{2-}$ dianion (see also Fig. 9).

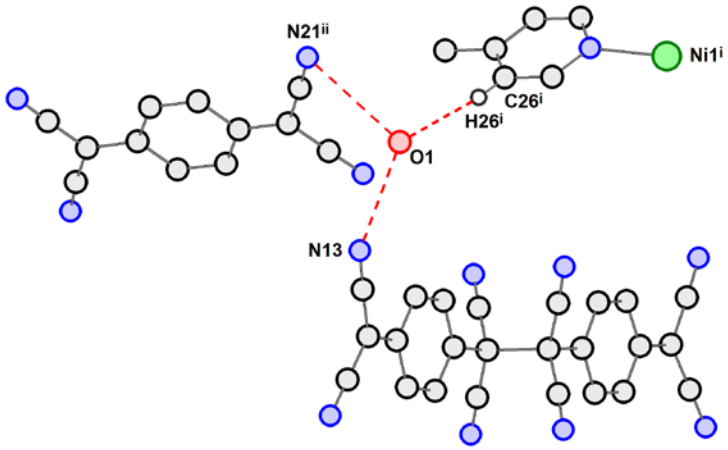

Fig. 11 Possible hydrogen bonding interactions (dashed lines) of the O1 water solvate molecule in **3**. Symmetry codes: i: 1-x, 1-y, 1-z; ii: 2-x, 1-y, 1-z.

hydrogen bonding interactions of the C-H···N type (Table S2, Fig. S4) linking the TCNQ with the complex cations. In addition, within this crystal structure π–π-stacking interactions link both of the crystallographically independent complex cations, plus TCNQ1 and TCNQ2 anion-radicals into a chain-like supramolecular structure (Fig. 12). The respective distances between the centroids are: $Cg1\cdots Cg6^{i}$, $Cg2\cdots Cg5^{i}$, $Cg3^{vii}\cdots Cg6^{i}$, $Cg4^{vi}\cdots Cg5^{i}$ 3.7731(2), 3.7283(2),

3.6162(2) and 3.7690(2) Å, respectively (Cg1, Cg2, Cg3 and Cg4 are the centroids of the pyridine rings containing N2, N4, N9 and N11, while Cg5 and Cg6 are the centroids of the quinoide rings of the TCNQ1 and TCNQ2 anion-radicals, respectively).

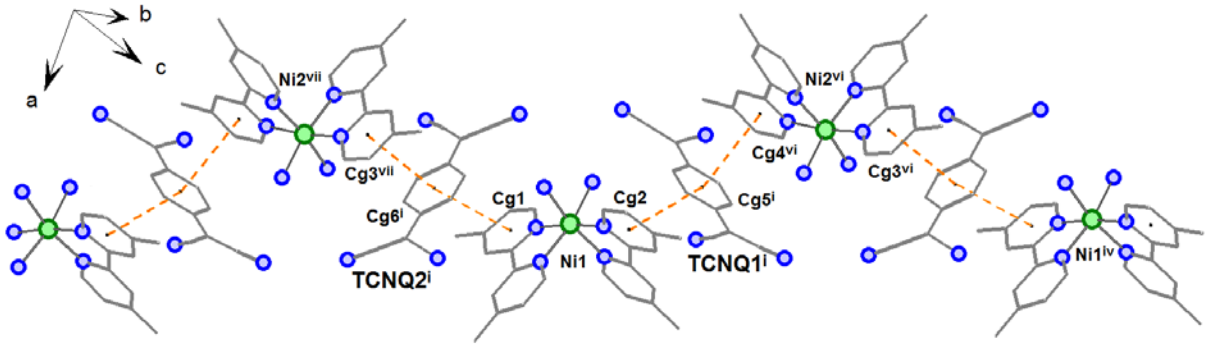

Fig. 12 Supramolecular chain-like arrangement of complex cations, TCNQ1 and TCNQ2 anion-radicals in **3**. Dashed lines represent contacts between the centres of gravity of the respective rings. Symmetry codes: i: 1-x, 1-y, 1-z; iv: x-1, y, z+1; vi: x-1, y, z; vii: x, y, z-1.

Magnetic properties

The magnetic properties were studied for **1** and **3** which could be prepared as separate phases. The temperature dependence of the magnetic susceptibility of **1** increases with decreasing temperature (Fig. 14). No difference between the susceptibility of the zero-field cooled (ZFC) and field cooled (FC) sample was observed. Susceptibility was fitted first by the Curie-Weiss law in the temperature range from 130 K to 300 K and the value of the Weiss temperature is -36.7 K. Temperature dependence of χ.T (Fig. 14) decreases from 1.92 emu.K/mol at a temperature of 300 K to 1.14 emu.K/mol at 1.8 K. The field dependence of magnetization was measured in magnetic fields of up to 7 T at 1.8 K and 5 K and exhibits no hysteresis (Fig. 15).

It is often difficult to obtain the correct sign for small values of the ZFS parameters from the analysis of the susceptibility and magnetization measured on polycrystalline samples. To avoid such ambiguity simple *ab initio* calculations using the ORCA package on the $[Ni(5,5'\text{-}dmbpy)_3]^{2+}$ cation from **1** and the two crystallographically independent $[Ni(4,4'\text{-}dmbpy)_3]^{2+}$ cations from **3** using the atomic coordinates obtained from single crystal X-ray data were performed. ZFS parameters calculated using the effective Hamiltonian theory are summarized

in Table 5. Similar ZFS parameters were obtained for [Ni(*bpy*)$_3$](B*Ph*$_4$)$_2$ [55]. Based on the structural parameters it is also possible to estimate ZFS parameters using the method of Baran et al. [56], but such a result is accurate for exact tetragonal or rhombic deformation of an ideal octahedron. Due to the significant deviations of all N-Ni-N angles from ideal values in **1** and **3** no conclusive estimations of ZFS parameters was possible.

Table 5 Results of ZFS parameters calculation using ORCA with effective Hamiltonian theory.

Cation	D/k_B (K)	E/D	g_{avg}
[Ni(5,5'-*dmbpy*)$_3$]$^{2+}$ (**1**)	-3.03	0.045	2.172
Ni1 in [Ni(4,4'-*dmbpy*)$_3$]$^{2+}$ (**3**)	-2.94	0.148	2.171
Ni2 in [Ni(4,4'-*dmbpy*)$_3$]$^{2+}$ (**3**)	-2.70	0.217	2.171

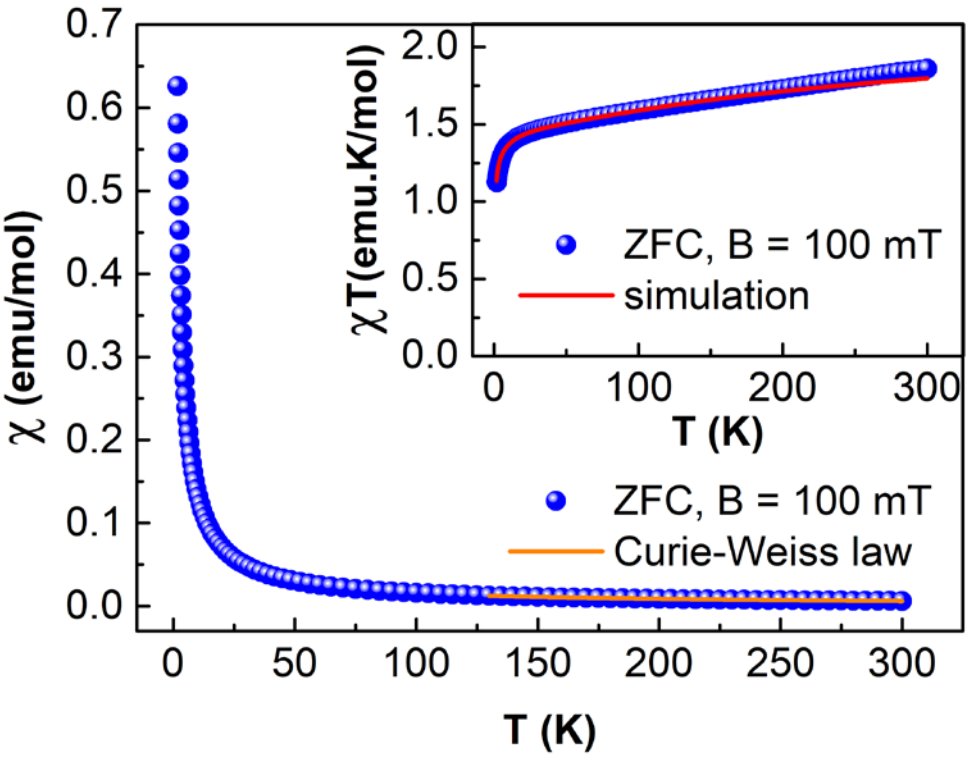

Fig. 14 The temperature dependence of magnetic susceptibility and χT (inset) for **1**.

For the analysis of experimental susceptibility, a model described by the equation:

$$\chi = \chi_{1chain} + \chi_{2chain} + \chi_{Ni} + \chi_{TIP}$$

was used, which includes the contributions of the paramagnetic Ni^{2+} ions with spin $S = 1$ and ZFS parameter D (χ_{Ni}) [57], two types of spin chains (χ_{1chain} and χ_{2chain}), represented by the Bonner-Fisher formula [58] and the contribution of the temperature independent paramagnetism (χ_{TIP}). One chain is formed by coupled TCNQ1 units (Fig. 3) where a structural dimer of $TCNQ^{\cdot-}$ anion-radicals has spin $S = 1/2$ within the supramolecular chain running in the direction of the *b* axis (Fig. 3). The other one consists of $TCNQ^{\cdot-}$ anion-radicals TCNQ2 where each single anion-radical carries spin $S = 1/2$ as indicated from bond lengths in the TCNQ molecule [51]. The best fit of the model to the susceptibility data for **1** yields the following parameters: $D/k_B = 2.5$ K, *g*-factors $g_{Ni} = 2.35$ and $g_{TCNQ} = 2$, exchange interaction within chains $J/k_B = -270$ K and $J/k_B = -70$ K and weak exchange interaction between Ni^{2+} ions $J/k_B = -0.3$ K (the negative value corresponds to an antiferromagnetic exchange interaction). A small deviation of the simulation in the high-temperature region may be caused by inaccurate subtraction of the diamagnetic contribution using Pascal's constants. A simulation of the field dependence of magnetization shown in Fig. 15 takes into account a spin chain with $J/k_B = -8.7$ K (calculated by the exact diagonalization of a spin ring with 10 spins) and a paramagnetic contribution of the Ni^{2+} ions with the same parameters as used for the magnetic susceptibility. The contribution of the spin chain with much stronger exchange $J/k_B = -157$ K is negligible at 1.8 K.

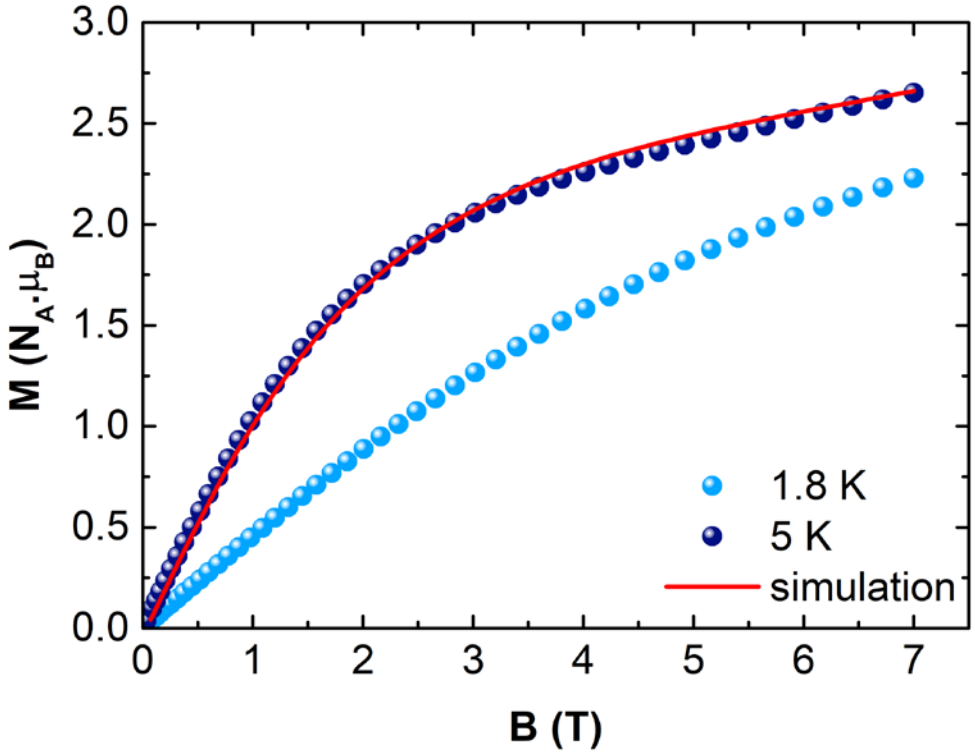

Fig. 15 The field dependence of isothermal magnetization at 1.8 K and 5 K for **1** (full symbols) including the simulation described in the text (solid line).

The magnetic susceptibility of **3** increases with decreasing temperature in the whole temperature range and no difference in ZFC and FC regimes was observed (Fig.16). The magnetic susceptibility was fitted by the Curie-Weiss law with Weiss temperature -12.3 K in the temperature range from 130 K to 300 K. The temperature dependence of χ.T decreases from 2.89 emu.K/mol at 300 K and shows a maximum at temperatures below 20 K (Fig. 16), which suggest weak interaction between the Ni^{2+} ions. The effective magnetic moment was estimated as 4.81 μ_B at 300 K and corresponds to two spins S = 1 from Ni^{2+} in the cations and two spins S = 1/2 from the independent $TCNQ^{\cdot-}$ anion-radicals. The anion-radicals bonded by a σ-bond, i.e., dianionic $(TCNQ\text{-}TCNQ)^{2-}$, have only a diamagnetic contribution to the magnetic properties [59-60]. The field dependence of magnetization exhibits no hysteresis and the magnetization is not saturated in a magnetic field of 7 T at a temperature of 5 K (Fig. 17).

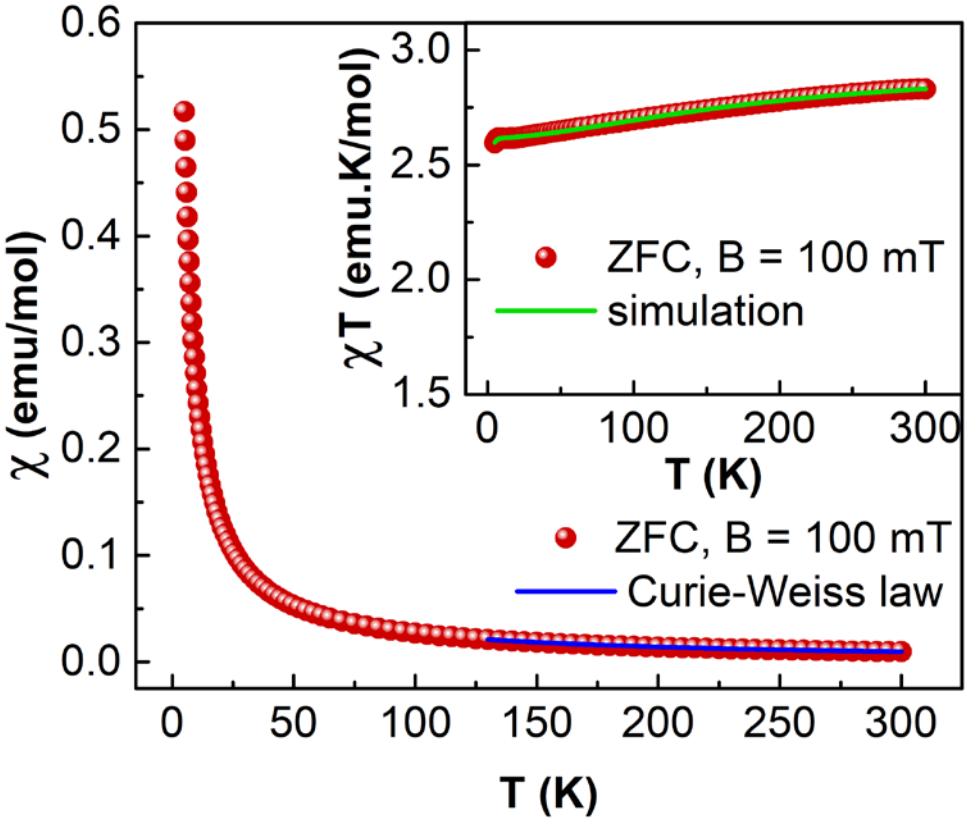

Fig. 16 The temperature dependence of magnetic susceptibility and χT (inset) for **3**.

Based on the crystal structure, experimental data of **3** were analysed by a model

$$\chi = \chi_{chain} + 2\chi_{Ni} + \chi_{C-W}$$

including the contributions of Ni^{2+} ions with spin S = 1 and ZFS parameter D (χ_{Ni}) [57], spin chain (χ_{chain}) [57] and the paramagnetic contribution from one of the crystallographically independent $TCNQ^{\cdot-}$ anion-radical (χ_{C-W}). We considered that the σ–dimerized $(TCNQ\text{-}TCNQ)^{2-}$ dianion is effectively in a singlet state [28]. Its charge density could mediate strong exchange interactions between crystallographically independent $TCNQ^{\cdot-}$ anion-radicals in the stack forming a spin chain. The best results of the simulation of magnetic properties for **3** was achieved for D/k_B = -4 K, g-factors g_{Ni} = 2.105 and g_{TCNQ} = 2, exchange interaction in the chain J/k_B = -164 K and weak exchange interaction between Ni^{2+} ions J/k_B = 0.25 K. Inclusion of a Weiss temperature of θ = -0.07 K for the paramagnetic contribution from one of the crystallographically independent $TNCQ^{\cdot-}$ anion-radicals suggests also the presence of a weak exchange interaction between them.

The low-temperature magnetization at maximum field in **3** is close to that expected for two Ni^{2+} ions and one paramagnetic anion-radical $TCNQ^{\cdot-}$ close to saturation, which again suggests the presence of relatively strong antiferromagnetic exchange interactions between TCNQ species in the stacks forming the chains.

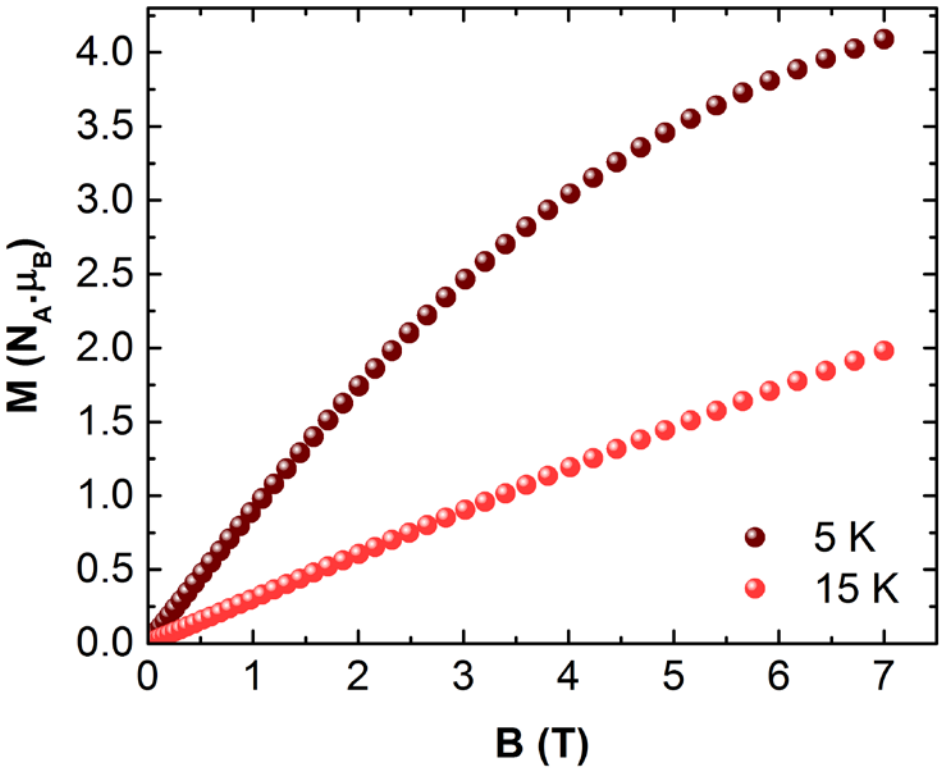

Fig. 17 The field dependence of isothermal magnetization at 5 K and 15 K for **3**.

4. Conclusions

In conclusion, three Ni(II) complexes with TCNQ, namely [Ni(5,5'-*dmbpy*)$_3$](TCNQ)$_2$ (**1**), [Ni(4,4'-*dmbpy*)$_3$](TCNQ)$_2$ (**2**), and [Ni(4,4'-dmbpy)$_3$]$_2$(TCNQ-TCNQ)(TCNQ)$_2$·0.60H_2O (**3**), were isolated and chemically characterized. All three compounds exhibit ionic crystal structures and their cationic parts are formed by tris(chelate) complex cations [Ni(5,5'-*dmbpy*)$_3$]$^{2+}$ and [Ni(4,4'-*dmbpy*)$_3$]$^{2+}$, respectively. While in **1** and **2** only $TCNQ^{\cdot-}$ anion-radicals form the anionic parts of the structures, in **3** the anionic part of the structure contains, in addition

to $TCNQ^{\cdot-}$ anion-radicals, a σ-dimerized $(TCNQ\text{-}TCNQ)^{2-}$ dianion. Measurements of magnetic susceptibility and magnetization of compounds **1** and **3** were performed. The presence of different types of TCNQ molecules in the crystal structures of **1** and **3** requires distinct and quite complicated models for the description of their magnetic properties.

Acknowledgment

Slovak grant agencies (APVV-14-0078, APVV-14-0073 and VEGA 1/0063/17) are acknowledged for the financial support of this work. The financial support from ERDF (European Regional Development Fund) under the contract Nos. ITMS26220120047 and ITMS26220220186 is acknowledged. Funding from the Spanish Ministry of Economy and Competitivity, Grant MAT2015-68200-C2-1-P with FEDER support, is acknowledged. We thank Dr. Beatriz Diosdado from the University of Zaragoza for X-ray data collection of complex **2**. One of the authors (LV) thanks P. J. Šafárik University in Košice (Slovakia) for financial support of her post-doctoral position.

Supporting data

CCDC 1576078-1576080 contain the supplementary crystallographic data for complexes **1-3**. These data can be obtained free of charge via http://www.ccdc.cam.ac.uk/conts/retrieving.html, or from the Cambridge Crystallographic Data Centre, 12 Union Road, Cambridge CB2 1EZ, UK; fax: (þ44) 1223-336- 033; or e-mail: deposit@ccdc.cam.ac.uk

References

[1] S.-S. Bao, L.-M. Zheng, Coord. Chem. Rev, 319 (2016) 63-85.

[2] G.A. Craigh, M. Murrie, Chem. Soc. Rev., 44 (2015) 2135-2147.

[3] H.L.C. Feltham, S. Brooker, Coord. Chem. Rev., 276 (2014) 1-33.

[4] S. Dhers, H.L.C. Feltham, S. Brooker, Coord. Chem. Rev., 296 (2015) 24-44.

[5] H. Fukunaga, H. Miyasaka, Angew. Chem. Int. Ed., 54 (2015) 569-573.

[6] G.-X. Liu, H. Xu, X.-M. Ren, W.-Y. Sun, Cryst. Eng. Comm., 10 (2008) 1574-1582.

[7] M. T. Azcondo, L. Ballester, L. Calderón, A. Gutiérrez, M. F. Perpinan, Polyhedron, 14 (1995) 2339–2347.

[8] G. Y. Vasylets, V. A. Starodub, B. Barszcz, A. Graja, V. V. Medviediev, O. V. Shishkin, A. S. Bukrinev, Synth. Metals, 191 (2014) 89–98.

[9] D. S. Acker, W. R. Hertler, J. Am. Chem. Soc., 84 (1962) 3370-3374.

[10] W. Kaim, M. Moscherosch, Coord. Chem. Rev., 129 (1994) 157-193.

[11] L. Ballester, A. Gutiérrez, M. F. Perpiñán, U. Amador, M. T. Azcondo, A. E. Sánchez, C. Bellitto, Inorg. Chem., 36 (1997) 6390–6396.

[12] L. Ballester, A. Gutiérrez, M. F. Perpiñán, M. T. Azcondo, Coord. Chem. Rev., 190-192 (1999) 447–470.

[13] J. P. Cornelissen, J.H. van Diemen, L. R. Groeneveld, J. G. Haasnoot, A. L. Spek, J. Reedijk, Inorg. Chem. 31 (1992) 198–202.

[14] P. J. Kunkeler, P. J. van Koningsbruggen, J. P. Cornelissen, A. N. van der Horst, A. M. van der Kraan, A. L. Spek, J. G. Haasnoot, J. Reedijk, J. Am. Chem. Soc., 118 (1996) 2190–2197.

[15] A. Nafady, A.P. O'Mullane, A.M. Bond, Coord. Chem. Rev., 268 (2014) 101-142.

[16] Z.-X. Wang, X. Zhang, Y.-Z. Zhang, M.-X. Li, H.-H. Zhao, M. Andruh, K. R. Dunbar, Angew. Chem. Int. Ed., 53 (2014) 11567-11570.

[17] N. Abdurakhmanova, T.-C. Tseng, A. Langner, C. S. Kley, V. Sessi, S. Stepanow, K. Kern, Phys. Rev. Lett., 110 (2013) Art. N. 027202.

[18] X. Zhang, H. M. Xie, M. Ballesteros-Rivas, T. J. Woods, K. R. Dunbar, Chem.-Eur. J., 23 (2017) 7448-7452.

[19] D. Dressel, Naturwissensch., 94 (2007) 527-541.

[20] V.A. Starodub, T.N. Starodub, Russ. Chem. Rev., 83 (2014) 391-438.

[21] I. Tascioglu, O. T. Ozmen, H. M. Sagban, E. Yaglioglu, S. Altindal, J. Electron. Mat., 46 (2017) 2379-2386.

[22] Y. N. Shvachko, D. V. Starichenko, A. V. Korolyov, A. I. Kotov, L. I. Buravov, V. N. Zverev, S. V. Simonov, L. V. Zorina, E. B. Yagubskii, Magnetochem., 3 (2017) Art. N. 9.

[23] F. Hoshyargar, M. Shafiei, C. Piloto, N. Motta, A. P. O'Mullane, J. Mat. Chem. C, 4 (2016) 11173-11179.

[24] H. Shiozawa, B. C. Bayer, H. Peterlik, J. C. Meyer, W Lang, T. Pichler, Sci. Rep., 7, (2017) Art. N.: 2439.

[25] S. K. Bhardwaj, A. L. Sharma, N. Bhardwaj, M. Kukkar, A. A. S. Gill, K. H. Kim, A. Deep, Sens. Actuat. B-Chem., 240 (2017) 10-17.

[26] M. Mohammadtaheri, R. Ramanathan, V. Bansal, Cat. Today, 278 (2016) 319-329.

[27] C. Fang, Y. Huang, L. X. Yuan, Y. J. Liu, W. L. Chen, Y.Y. Huang, K.Y. Chen, J.T. Han, Q. J. Liu, Y. H. Huang, Angew. Chem.-Int. Ed., 56 (2017) 6793-6797.

[28] C. Alonso, L. Ballester, A. Gutiérrez, M. F. Perpiñán, A. E. Sánchez, M. T. Azcondo, Eur. J. Inorg. Chem., (2005) 486-495.

[29] L. Ballester, M. C. Barral, A. Gutiérrez, A. Monge, M. F. Perpiñán, C. Ruiz-Valero, E. Sánchez-Pélaez, Inorg. Chem.**,** 33 (1994) 2142–2146.

[30] J. Černák, I. Kočanová, M. Orendáč, Comm. Inorg. Chem., 33 (2012) 2-54.

[31] J. Černák, J. Kuchár, M. Hegedüs, Acta Crystallogr., E73 (2017) 8-12.

[32] L. R. Melby, R. J. Herder, W. Mahler, R. E. Benson, W. E. Mochel, J. Am. Chem. Soc., 84 (1962) 3374–3387.

[33] Oxford Diffraction. CrysAlis RED and CrysAlis CCD software (Ver. 1.171.38.41). Rigaku Oxford Diffraction Ltd. Abingdon, Oxfordshire, England (2015).

[34] R.C. Clark, J.S. Reid, Acta Crystallogr., A51 (1995) 887-897.

[35] G.M. Sheldrick, Acta Cryst., A64 (2008) 112-122.

[36] G.M. Sheldrick, Acta Cryst., C71 (2015) 3-8.

[37] L.J. Farrugia, J. Appl. Cryst., 45 (2012) 849-854.

[38] R.H. Blessing, Acta Crystallogr., B51 (1995) 816-823.

[39] R.H. Blessing, J. Appl. Crystallogr., 30 (1997) 421-426.

[40] M. C. Burla, R. Caliandro, B. Carrozzini, G. L. Cascarano, C. Cuocci, C. Giacovazzo, M. Mallamo, A. Mazzone, G. Polidori, J. Appl. Cryst., 48 (2015) 306-309.

[41] A. L. Spek, Acta Crystallogr., C71 (2015) 9-18.

[42] K. Brandenburg, DIAMOND. Crystal Impact (version 3.1f) GbR, Bonn, Germany, 2008.

[43] G. A. Bain, J. F. Berry, J. Chem. Educ., 85 (2008) 532-536.

[44] (a) F. Neese, Rev. Comput. Mol. Sci., 2 (2012) 73; (b) F. Neese, ORCA − An Ab Initio, DFT and SCF-MO Program Package, Version 4.0.1; (c) M. Atanasov, D. Ganyushin, D. A. Pantazis, K. Sivalingam, F. Neese, F., Inorg. Chem., 50 (2011) 7460; (d) C. Angeli, S. Borini, M. Cestari, R. Cimiraglia, J. Chem. Phys., 121 (2004) 4043; (e) C.

Angeli, R. Cimiraglia, S. Evangelisti, T. Leininger, J.-P. Malrieu, J. Chem. Phys., 114 (2001) 10252; (f) C. Angeli, R. Cimiraglia, J.-P. Malrieu, J. Chem. Phys., 117 (2002) 9138; (g) F. Neese, J. Chem. Phys., 122 (2005) 034107; (h) D. Ganyushin, F. Neese, J. Chem. Phys., 125 (2006) 024103; (i) F. Neese, J. Chem. Phys., 127 (2007) 164112.

[45] N. Thuyweang, L. L. Koh, T. S. A. Hor, S. Leelasubcharoen, J. Coord. Chem., 67 (2014) 1219-1235.

[46] J. Breu, H. Domel, A. Stoll, Eur. J. Inorg. Chem., (2000) 2401-2408.

[47] C. R. Groom, I. J. Bruno, M. P. Lightfoot, S. C. Ward, Acta Cryst., B72 (2016) 171-179.

[48] Y. Liu, R. Zhan, Z. Han., K. Gong, X. He, X. Zhai, J. Sol. St. Chem., 231 (2015) 169-174.

[49] M. Ballesteros-Rivas, A. Ota, E. Reinheimer, A. Prosvirin, J. Valdés-Martinez, K. R. Dunbar, Angew. Chem. Int. Ed., 50 (2011) 9703–9707.

[50] J. Huang, S. Kingsbury, M. Kertesz, Phys. Chem. Chem. Phys., 10 (2008) 2625-2635.

[51] T. J. Kistenmacher, T. J. Emge, A. N. Bloch, D. O. Cowan, Acta Crystallogr., B38 (1982) 1193−1199.

[52] C. Anderer, N. D.de Alarcon, C. Nather, W. Bensch, Chem.-Eur. J., 20 (2014) 16953–16959.

[53] S. Shimomura, M. Higuchi, R. Matsuda, K. Yoneda, Y. Hijikata, Y. Kubota, Y. Mita, J. Kim, M. Takata, S. Kitagawa, Nature Chem., 2 (2010) 633-637.

[54] V. Dong, H. Endres, H. J. Keller, W. Moroni, D. Nöthe, Acta Crystallogr., B33 (1977) 2428-2431.

[55] G. Charron, E. Malkin, G. Rogez, L. J. Batchelor, S. Mazerat, R. Guillot, N. Guihéry, A-L. Barra, T. Mallah, H. Bolvin, Chem. Eur. J., 22 (2016) 16850-16862.

[56] a) P. Baran, M. Boča, R. Boča, A. Krutošíková, J. Miklovič, J. Pelikán, J. Titiš, Polyhedron 24 (2005) 1510–1516; b) R. Ivaniková, R. Boča, L. Dlháň, H. Fuess, A. Mašlejová, V. Mrázová, I. Svoboda, J. Titiš, Polyhedron, 25 (2006) 3261-3268.

[57] O. Kahn, Molecular magnetism, VCH Publishers, Inc. New York, 1993.

[58] 53 J. C. Bonner, M. E. Fisher, Phys. Rev., 135 (1964) A640-A658.

[59] 56 H. Zhao, R. A. Heintz, X. Ouyang, K. R. Dunbar, C. F. Campana, R. D. Rogers, Chem. Mater., 11 (1999) 736-746.

[60] 57 S. Mikami, K. Sugiura, J.S. Miller, Y. Sakata, Chem. Lett., 28 (1999) 413-414.

Appendix A. Supplementary data

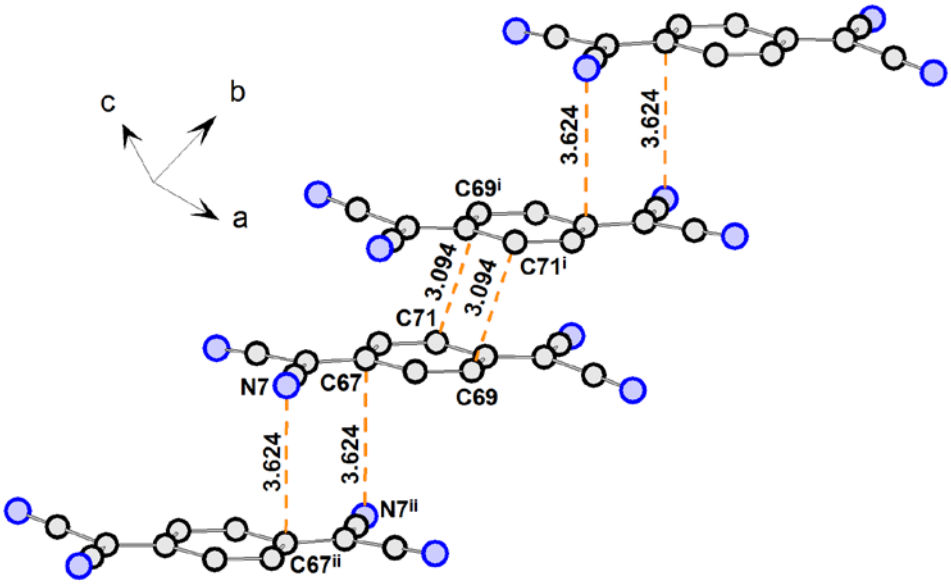

Fig. S1 Chain-like arrangement of TCNQ1 anion-radicals in the crystal structure of **1**. Dashed lines represent the shortest contacts between the neighbouring anion-radicals within the chain-like arrangement.

Table S1 Possible hydrogen bonding interactions in **1** in [Å,°].

D-H···A	D – H	H···A	D···A	D-H···A
C15-H15···N7^{ii}	0.95	2.53	3.1740(1)	125
C24-H24···N8^{iii}	0.95	2.59	3.4905(2)	159
C34-H34···N8^{iv}	0.95	2.61	3.5480(2)	168
C65-H65···N13^{v}	0.95	2.41	3.3533(1)	172

Symmetry codes: ii: 2-x, -y, 1-z; iii: 1-x, -y, 1-z; iv: x, 1+y, z; v: -x, y-0.5, 0.5-z

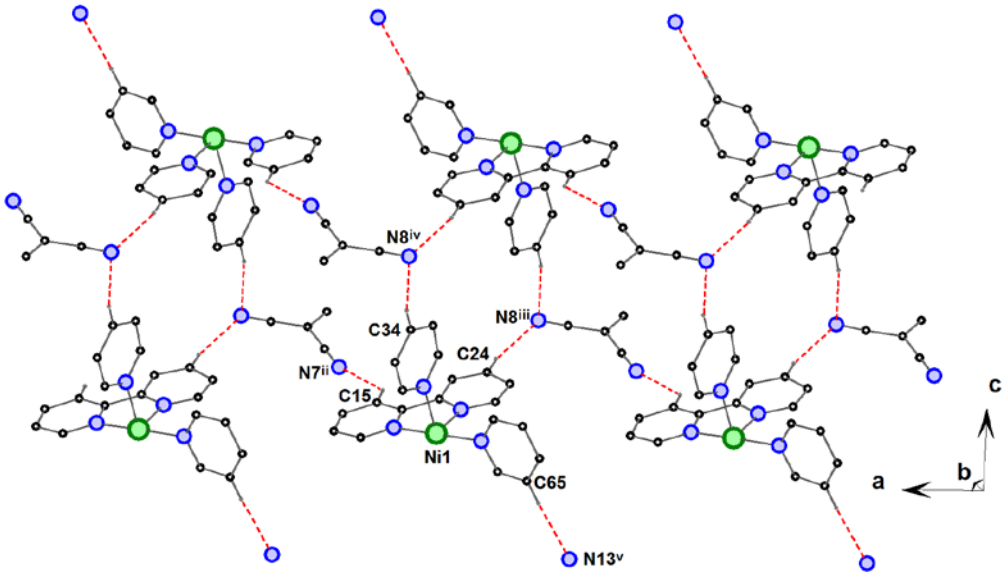

Fig. S2 View of the possible hydrogen bonding interactions in **1**. For the sake of clarity the hydrogen atoms not involved in interactions are omitted. For the complex cations and TCNQ anion radicals only atoms involved in hydrogen bonding interactions are displayed. Symmetry codes: ii: 2-x, -y, 1-z; iii: 1-x, -y, 1-z; iv: x, 1+y, z; v: -x, y-0.5, 0.5-z.

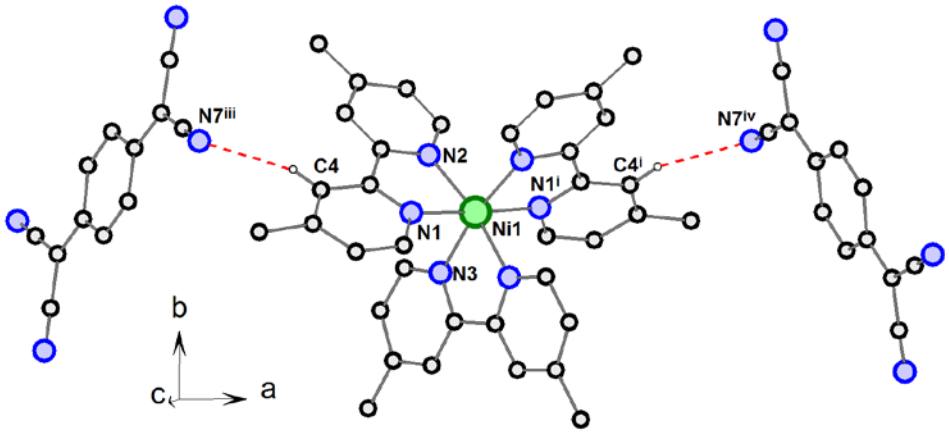

Fig. S3 Trimeric supramolecular unit of **2**. The dashed lines represent weak hydrogen bonding interactions of the C-H···N type.

Symmetry codes: i: 1-x, y, 0.5-z; ii: 1-x, 1-y, 1-z; iii: x-0.5, 0.5-y, z-0.5; iv: 1.5-x, 0.5-y, 1-z.

Table S2 Possible hydrogen bonding interactions in **3** in [Å, °].

D-H···A	D – H	H···A	D···A	D-H···A
C26-H26···O1^{i}	0.95	2.41	3.3082(2)	158
C9-H9···N27^{iii}	0.95	2.35	3.2844(2)	168
C11-H11B···N18	0.98	2.55	3.4998(2)	163
C12-H12B···N17	0.98	2.56	3.4210(2)	147
C13-H13···N14	0.95	2.60	3.2734(2)	128
C16-H16···N20^{iv}	0.95	2.49	3.4272(2)	169
C24-H24A···N26	0.98	2.61	3.5071(2)	152
C45-H45···N28^{v}	0.95	2.61	3.5297(2)	162
C59-H59A···N24^{i}	0.98	2.51	3.4806(2)	170
C59-H59C···N15^{iv}	0.98	2.60	3.5506(2)	164
C60-H60B···N16^{iv}	0.98	2.59	3.5585(2)	172
C64-H64···N13	0.95	2.59	3.5162(2)	166
C67-H67···N13	0.95	2.48	3.4260(2)	175

i: 1-x, 1-y, 1-z; iii: x, 1+y, z-1; iv : x-1, y, 1+z ; v : x, 1+y, z.

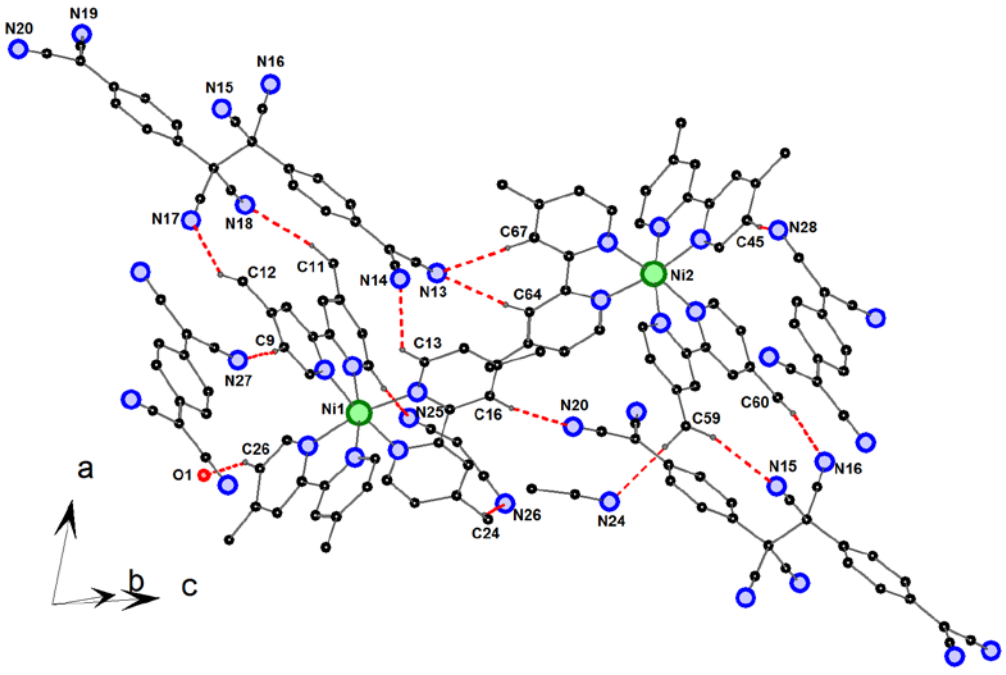

Fig. S4 View of the possible hydrogen bonding system in **3**. The dashed lines represent weak hydrogen bonding interactions of the C-H···N and C-H···O types.

Symmetry codes: i: 1-x, 1-y, 1-z; iii: x, 1+y, z-1; iv: x-1, y, 1+z ; v : x, 1+y, z.